



HAL
open science

NAD kinases use substrate-assisted catalysis for specific recognition of NAD.

Guillaume Poncet-Montange, Liliane Assairi, Stefan Arold, Sylvie Pochet,
Gilles Labesse

► **To cite this version:**

Guillaume Poncet-Montange, Liliane Assairi, Stefan Arold, Sylvie Pochet, Gilles Labesse. NAD kinases use substrate-assisted catalysis for specific recognition of NAD.. *Journal of Biological Chemistry*, 2007, 282 (47), pp.33925-34. 10.1074/jbc.M701394200 . pasteur-00202295

HAL Id: pasteur-00202295

<https://pasteur.hal.science/pasteur-00202295>

Submitted on 27 May 2021

HAL is a multi-disciplinary open access archive for the deposit and dissemination of scientific research documents, whether they are published or not. The documents may come from teaching and research institutions in France or abroad, or from public or private research centers.

L'archive ouverte pluridisciplinaire **HAL**, est destinée au dépôt et à la diffusion de documents scientifiques de niveau recherche, publiés ou non, émanant des établissements d'enseignement et de recherche français ou étrangers, des laboratoires publics ou privés.



Distributed under a Creative Commons Attribution 4.0 International License

NAD Kinases Use Substrate-assisted Catalysis for Specific Recognition of NAD^{*}[§]

Received for publication, February 16, 2007, and in revised form, July 17, 2007. Published, JBC Papers in Press, August 8, 2007, DOI 10.1074/jbc.M701394200

Guillaume Poncet-Montange^{†§1}, Liliane Assairi^{§¶}, Stefan Arold^{†§}, Sylvie Pochet^{¶||}, and Gilles Labesse^{†§2}

From the [†]Atelier de Bio- et Chimie Informatique Structurale, Centre de Biochimie Structurale, UMR5048, CNRS, Universités Montpellier 1 et 2, 29 rue de Navacelles, F34090 Montpellier, France, [§]INSERM, U554, 29 rue de Navacelles, F34090 Montpellier, France, [¶]INSERM, U759, Institut Curie, 91405 Orsay, France, and ^{||}Unité de Chimie Organique, Institut Pasteur, CNRS, URA 2128, 75724 Paris, France

Here we describe the crystal structures of the NAD kinase (LmNADK1) from *Listeria monocytogenes* in complex with its substrate NAD, its product NADP, or two synthesized NAD mimics. We identified one of the NAD mimics, di-adenosine diphosphate, as a new substrate for LmNADK1, whereas we showed that the closely related compound di-5'-thioadenosine is a novel non-natural inhibitor for this enzyme. These structures suggest a mechanism involving substrate-assisted catalysis. Indeed, sequence/structure comparison and directed mutagenesis have previously shown that NAD kinases (NADKs) and the distantly related 6-phosphofruktokinases share the same catalytically important GGDGT motif. However, in this study we have shown that these enzymes use the central aspartate of this motif differently. Although this acidic residue chelates the catalytic Mg²⁺ ion in 6-phosphofruktokinases, it activates the phospho-acceptor (NAD) in NADKs. Sequence/structure comparisons suggest that the role of this aspartate would be conserved in NADKs and the related sphingosine and diacylglycerol kinases.

With the emergence of antibiotic resistance worldwide, the search for new antibacterial compounds has become increasingly important (1). NADKs³ represent an attractive and novel drug target for antibiotic discovery. Indeed, NADKs (EC 2.7.1.23) were recently shown to be essential for growth in many bacteria (2–4) including various human pathogens such as *Mycobacterium tuberculosis* (5), *Staphylococcus aureus* (6), *Streptococcus pneumoniae* (7), *Salmonella enterica* (8), and *Pseudomonas aeruginosa*.⁴ NADKs are ubiquitous enzymes

involved in the last step of the biosynthesis of NADP catalyzing the transfer of a phosphate group on the substrate NAD to produce NADP in the presence of both ATP and Mg²⁺. NADKs are also involved in the tight regulation of the NADH/NADPH ratio (8). Both NAD(P) and NAD(P)H are essential cofactors for a large number of enzymes involved in various metabolic pathways such as oxidoreductases. This activity of NADKs has been well known for decades, but their genes were cloned only recently (9), subsequently leading to rapid identification of NADK orthologs in many organisms from bacteria, Archaea, plants, and human (Pfam PF01513). Bacterial and human enzymes show significant functional and sequence divergences, and the NADK activity in human cells is low (10).

However, despite recent advances in the characterization of NADKs, the reaction mechanism is not well understood, and some original features of NADKs remain unexplained. First, during catalysis the phosphorylation occurs specifically on 2'-hydroxyl of the adenosine moiety of NAD and not on the neighboring 3'-hydroxyl. Second, the specificity for the catalytic di-cation is low (Mn²⁺, Ca²⁺, Zn²⁺, Co²⁺, and Fe²⁺ appear equivalent to Mg²⁺) (11), whereas it is generally high in other well characterized kinases. Furthermore, the di-cation binding motif is yet unknown. Finally, most NADKs use as a phospho-donor various nucleoside triphosphates (9, 12, 13). Polyphosphates can also act as a donor but only for NADKs from Gram(+) bacteria and from mycobacteria (9). On the contrary, the human NADK counterpart preferentially uses ATP (7% activity with GTP) (10).

The recent determination of the crystal structures of NADKs from *M. tuberculosis* and *Archaeoglobus fulgidus* unbound or in the presence of NAD or NADP allowed to more clearly locate the active site (14–16), but the precise reaction mechanism remained speculative (15).

We now report crystal structures of NADK from the human pathogen *Listeria monocytogenes* (LmNADK1) as a first representative of the enzymes from Gram(+) bacilli. The crystal structures of LmNADK1 ligand-free or in complex with its natural substrate or its product were solved at 2.3, 2.1, and 2.1 Å, respectively. Furthermore, we designed and synthesized two molecules mimicking NAD: di-adenosine diphosphate and di-5'-thioadenosine. Additionally, we characterized two mutants whose function, but not their structure, was affected.

Our analysis highlights important and previously unnoticed features of the NAD reaction mechanism. (i) We reveal the molecular basis for the 2'-hydroxyl specificity of NAD, (ii) we

* The costs of publication of this article were defrayed in part by the payment of page charges. This article must therefore be hereby marked "advertisement" in accordance with 18 U.S.C. Section 1734 solely to indicate this fact.

§ The on-line version of this article (available at <http://www.jbc.org>) contains supplemental Figs. S1–S7.

The atomic coordinates and structure factors (code 2I1W, 2I29, 2I2A, 2I2B, 2I2C, 2I2D, 2I2E, 2I2F, and 2Q5F) have been deposited in the Protein Data Bank, Research Collaboratory for Structural Bioinformatics, Rutgers University, New Brunswick, NJ (<http://www.rcsb.org/>).

¹ Present address: Université Montpellier 2 and INSERM, U710, Montpellier, F-34095 France and EPHE, Paris, F-75007 France.

² To whom correspondence should be addressed. Tel.: 33-4-67-41-77-12; Fax: 33-4-67-41-79-13; E-mail: labesse@cbs.cnrs.fr.

³ The abbreviations used are: NADK, NAD kinase; LmNADK1, NADK1 from the *L. monocytogenes*; Ap2A, di-adenosine diphosphate; TAA, 5'-thioacetyl-adenosine; DTA, di-(5'-thioadenosine); PFK, phosphofruktokinase; HPLC, high performance liquid chromatography.

⁴ M. A. Jacobs, J. M. Urbach, and F. M. Ausubel, personal communication.

Substrate-assisted Catalysis of NAD Kinases

show that NADKs and the structurally related phosphofructokinases (PFKs) use the same catalytic GGDGT motif in a different manner, and (iii) we suggest that the diphosphate group of the substrate plays the role of a di-cation chelator, revealing a mechanism involving substrate-assisted catalysis.

EXPERIMENTAL PROCEDURES

Chemicals, Bacterial Strains, Plasmids—The oligonucleotides were synthesized by MWG-Biotech. The restriction enzymes were purchased from Biolabs and Roche Applied Science. *Vent* DNA polymerase and *Tfu* DNA polymerase were from Qbiogene, and T4 DNA ligase was purchased from Biolabs. Isopropyl- β -D-1-thiogalactopyranoside was from ICN Biomedical Inc. Isocitrate dehydrogenase from porcine heart, sodium isocitrate, NAD, and nucleosides triphosphates were from Sigma or Roche Applied Science. The kits used for plasmid preparation were from either Sigma or Macherey-Nagel. Genomic DNA of *L. monocytogenes* strain EGD-e was a gift of P. Cossart (Institut Pasteur). The *Escherichia coli* strains NM554 and BL21(DE3)/pDIA17 were purchased from Stratagene and Novagen.

Cloning, Site-directed Mutagenesis, and Expression in *E. coli*—The NAD kinase 1 (EC 2.7.1.23) coding sequence was amplified by PCR from the genomic DNA isolated from *L. monocytogenes* strain EGD-e by using the *Vent* DNA polymerase, dNTPs, and the following primers: 5'-Lm, 5'-GGAATTCATATGAAATATATGATTACTTCCAAAGGA-3', and 3'-Lm, 5'-CGGCGCTCGAGTTAATCTTCAATAAACGAATCGTGTAC-3'. The amplified DNA was cloned into the expression vector pET22b (Novagen) at the NdeI and XhoI restriction sites (underlined) giving the following plasmid pLA15.3.3. Site-directed mutagenesis was performed using the double PCR method by using the *Tfu* DNA polymerase the two above primers and the following mutagenic primers: D45N, 5'-AGACAGAAATGTTCCATTGCCACCAATAGAAAT-3', and H223E, 5'-ATGCAAAATGCTCAGCTCGTCTACAGAAATTTG-3'. The final PCR products were purified and cloned into the pET22b vector at the NdeI and XhoI restriction sites. The mutated genes were sequenced, and the corresponding plasmids were then used for transforming the *E. coli* strain BL21(DE3)/pDIA17 for protein expression.

The transformants were grown at 37 °C in 2YT medium (Difco) in the presence of chloramphenicol and ampicillin at 30 μ g/ml. When the absorbance reached 1.5 at 600 nm, the expression of the both recombinant proteins was then induced by the addition of 1 mM isopropyl- β -D-1-thiogalactopyranoside, and growth was continued for three more hours at 37 °C. The cells were then pelleted by centrifugation and served as source for protein purification. For production of the selenomethionine derivative, selenomethionine was incorporated in place of methionine, whereas the cells were grown in M9 minimum media supplemented with 20 mM glucose, 2 mM magnesium sulfate, ampicillin (30 μ g/ml), and chloramphenicol (30 μ g/ml) at 37 °C. When the absorbance at 600 nm reached 0.5, the medium was supplemented with the amino acids lysine, threonine, and phenylalanine at 100 mg/ml and leucine, isoleucine, valine, and selenomethionine at 50 mg/ml. After 30 min the expression was induced by the addition of 0.5 mM isopro-

pyl- β -D-1-thiogalactopyranoside for 16 h at 37 °C. Soluble protein was purified using cobalt-agarose affinity chromatography followed by size exclusion chromatography. The protein was concentrated to 6–7 mg/ml in 25 mM sodium acetate, pH 5.2. The mutants were produced as described above for the wild-type enzyme and showed similar characteristics as monitored by SDS/PAGE, dynamic light scattering, and circular dichroism (data not shown).

Enzymatic Assay—The NAD kinase activity was determined by measuring the NADP produced by using isocitrate dehydrogenase as a coupling enzyme. Kinetic parameters for ATP were obtained by fitting data to the Michaelis-Menten equation. Kinetics parameters for NAD were obtained by fitting data to the Hill equation. For determination of ADP produced, enzyme was incubated in 50 mM sodium phosphate, pH 7.5, 100 mM NaCl, 10 mM MgCl₂ with substrates or inhibitors at various concentrations for 30 min at 30 °C. Cobalt resin was added to the sample for removal of the protein and centrifuged. The supernatant was tested for ADP production in 50 mM Tris-HCl, pH 7.4, 50 mM KCl, 1 mM phosphoenolpyruvate, 0.2 mM NADH, and 2 units each of lactate dehydrogenase and pyruvate kinase, and the decrease of absorbance was measured at 340 nm at 30 °C using a spectrophotometer Eppendorf ECOM 6122. Phosphorylation of di-5'-thioadenosine (DTA) was tested at rather high concentrations of substrate (3 mM) due to the low overall activity (no activity detected at 1 mM) of the wild-type and mutant enzymes.

Crystallization—Initial crystallization conditions of LmNADK1 were found by using a hanging-drop-based sparse-matrix screening strategy. The best crystals were obtained by mixing 1 μ l of the protein solution (concentration 11–15 mg/ml) with an equal volume of crystallization buffer (0.3 M potassium chloride, 50 mM trisodium citrate dihydrate, pH 5.6, 15–20% w/v polyethylene glycol 400) equilibrated over 0.5 ml of the same buffer. Two independent crystal forms were grown in nearly identical conditions in the presence of 10 mM iodine (apo structure, space group P2₁) or in the presence (holo structure, space group I222) of 10 mM 5'-thioacetyladenosine (TAA, Fig. 1C). The complexes with bound NAD, NADP, and NAD mimics were solved using crystals in the orthorhombic form. After growing them in presence of TAA, crystals were washed in the mother liquor and soaked with millimolar concentration of the desired ligand in a preequilibrated hanging drop.

Crystallographic Studies—X-ray diffraction data sets were collected from frozen single crystals at the European Synchrotron Radiation Facility (Grenoble, France, beamlines BM30A, ID14, and ID23) and processed with the programs MOSFLM, SCALA, and TRUNCATE from the CCP4 program suites (18) (Tables 1 and 2). The structure was solved by using a multiple wavelength anomalous diffraction experiment from a highly redundant 4- \AA data set of the selenomethionine-labeled protein. Twenty-two of 24 selenium sites were found by direct methods with the program SHAKE'N'BAKE (19) and refined with the program SHARP (20). Electron density modification was performed with SOLOMON (20). A molecular replacement solution was obtained using the program PHASER (21) and the crystal structure PDB code 1U0R (14). Phases derived from multiwavelength anomalous diffraction data and from

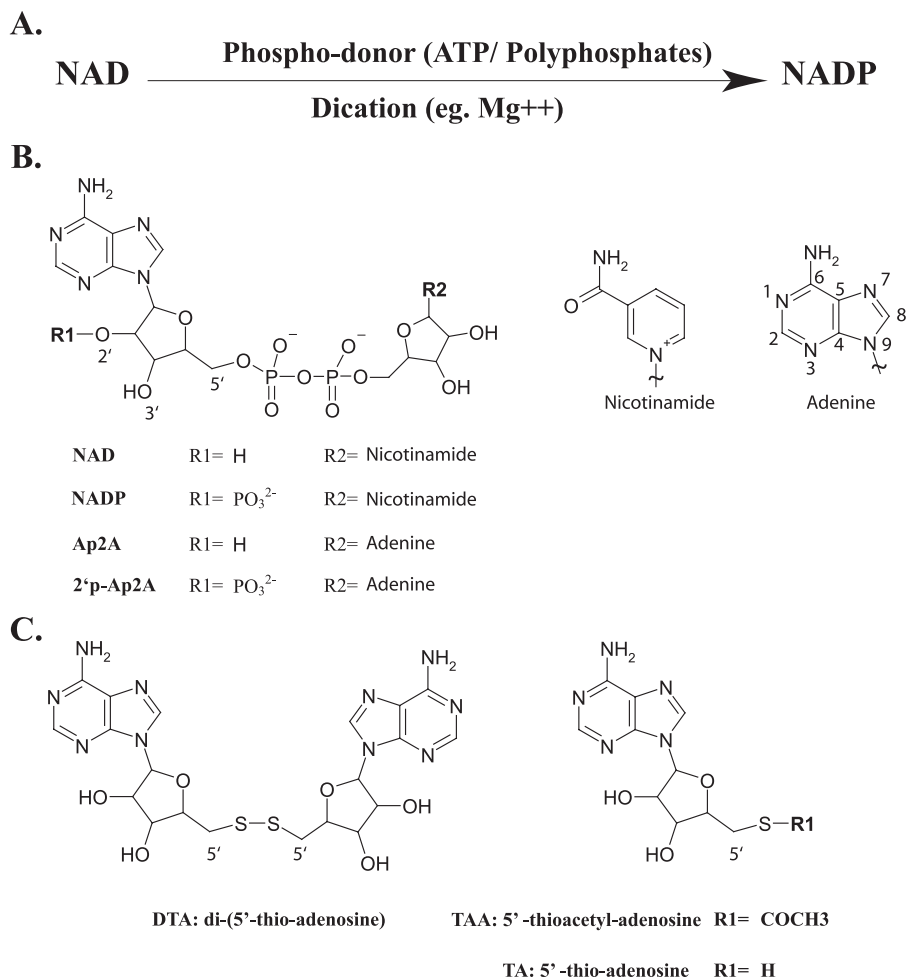


FIGURE 1. **Schematic reaction and chemical structures of nucleotides described in this study.** A, schematic reaction of the NADKs. B, dinucleotides linked by a diphosphate group and representation of adenine and nicotinamide moiety. C, dinucleotide linked by a disulfide bridge (DTA) and its protected form (TAA).

molecular replacement were then combined using the program DMMULTI (22). 4-Fold NCS was applied in DMMULTI (22) and during the first steps of refinement in REFMAC5 as implemented in CCP4 (18). Iterative model rebuilding and refinement was performed first by using the program O (23) and then the program COOT (24) and the program REFMAC5 using a translation/libration/screw model (25) against the native data set at 2.4-Å resolution. In the final model short segments of the protein (loops 69-TGHL-72, 110-GIGKK-114, and 129-SGGP-132) are not clearly visible in the electron density map. Similarly, the last residue and/or the affinity tag (monomers A, C, and D) or the last five histidines (monomer B) could not be modeled.

Molecular replacement was performed to solve the first structure in orthorhombic form. Subsequent determinations were performed on isomorphous crystals. Refinement was performed using REFMAC5 using the same translation/libration/screw model. As in the case of the monoclinic form, some side chains and several short segments of the protein (mainly loops 69-TGHL-72, 110-GIGKK-114, and less frequently 129-SGGP-132) are not clearly visible in the electron density map. Similarly, the last residue and/or the affinity tag could not be modeled in most protein-ligand complexes. Figures of ligands and corre-

sponding electronic density were generated using PyMOL (DeLano Scientific).

Chemical Synthesis—Solvents were spectroscopic or HPLC grade. ¹H and ³¹P NMR spectra were recorded on a Bruker Avance 400 spectrometer operating at 400.13 MHz and 161.97 MHz, respectively. Preparative and analytical HPLC were carried out on a PerkinElmer Life Sciences system (200 Pump) using a C18 reverse phase column (Kromasil, particle size 5; pore size 100) at a flow rate of 5.5 or 1 ml/min and a linear gradient of CH₃CN in 20 mM triethylammonium acetate buffer at pH 7.5 over 20 min. Mass spectra were recorded at the mass spectroscopy laboratory (CNRS-ICSN, Gif-sur-Yvette).

TAA was synthesized from commercially available 2',3'-isopropylidene-adenosine and thioacetic acid under Mitsunobu conditions as previously described (17). The acetonide group was then removed in aqueous formic acid to yield after purification by silica gel chromatography TAA in a total yield of 60%. 5'-thioadenosine (Fig. 1C) was obtained from TAA by hydrolysis using a mixture of MeOH/H₂O saturated with ammonia under oxygen free conditions. The chemical structure of 5'-thioadenosine was confirmed by NMR and mass analysis, and its purity (absence of disulfide formation) was checked by reverse phase HPLC analysis and compared with DTA as control. Di-adenosine diphosphate (Ap2A, Fig. 1B) was prepared by condensation of 5'-phosphomorpholidate of adenosine (26) and adenosine 5'-monophosphate as the tributylammonium salt in anhydrous *N,N*-dimethylformamide. After purification by reverse phase HPLC, Ap2A was isolated as sodium salt in 50% yield.

of 5'-thioadenosine was confirmed by NMR and mass analysis, and its purity (absence of disulfide formation) was checked by reverse phase HPLC analysis and compared with DTA as control. Di-adenosine diphosphate (Ap2A, Fig. 1B) was prepared by condensation of 5'-phosphomorpholidate of adenosine (26) and adenosine 5'-monophosphate as the tributylammonium salt in anhydrous *N,N*-dimethylformamide. After purification by reverse phase HPLC, Ap2A was isolated as sodium salt in 50% yield.

RESULTS

Overall Structure and Topology—Two independent crystal forms were grown in nearly identical conditions in the absence (apo structure, space group P2₁) or in the presence of an adenosine analogue (holo structure, space group I222) named 5'-thioacetyladenosine (hereafter TAA, Fig. 1C). First, we determined the apo structure of LmNADK1 in the P2₁ crystal form. Initial molecular replacement trials using 2.4-Å resolution data from native P2₁ crystals and the structure of the mycobacterial NADK (14), which is only 24% identical in sequence to LmNADK1, yielded a solution with plausible crystal packing and a score above noise level. However, this model could not be easily refined. Structure determination was only successful

Substrate-assisted Catalysis of NAD Kinases

TABLE 1

Data collection, phasing, and refinement statistics for apo LmNADK1

SeMet, selenomethionine; a.u., asymmetric units.

	Native	SeMet peak	SeMet inflection	SeMet remote
Data collection				
Space group	P2 ₁		P2 ₁	
Cell dimension				
<i>a</i> , <i>b</i> , <i>c</i> (Å)	66.6, 119.0, 67.9		67.2, 119.3, 67.5	
β (°)	102.0		102.0	
No. molecules (in a.u.)	4		4	
Wavelength (Å)	0.9798	0.9797	0.9801	0.9778
Resolution (Å) ^a	34.5-2.34 (2.47-2.34)		57.5-4.00 (4.20-4.00)	
R_{merge} (%) ^{a,b}	6.6 (43.1)	5.0 (8.4)	4.6 (9.2)	4.5 (7.2)
$I/\sigma I^2$	13.9 (2.9)	18.9 (8.0)	18 (6.0)	20.1 (7.9)
Completeness (%) ^a	97.5 (99.3)	96.6 (77.7)	94.1 (68.4)	97.7 (85.2)
Redundancy ^a	3.6 (3.6)	3.4 (1.6)	2.9 (1.5)	3.4 (1.6)
B-wilson	49.9	31.6	44.9	39.7
Refinement				
Resolution (Å)	34.5-2.34			
No. Reflections	42,472			
$R_{\text{work}}/R_{\text{free}}$ (%) ^c	19.9/26.6			
No. atoms				
Protein	8194			
Iodide	18			
Water	362			
B-factors (Å ²)				
Protein	38.9			
Iodide	38.5			
Water	39.8			
Root mean square deviations ^d				
Bond lengths (Å)	0.010			
Bond angles (°)	1.23			

^a Values in parentheses refer to the outermost resolution shell.

^b $R_{\text{merge}} = \frac{\sum_{\text{hkl}} \sum_i |I_{\text{hkl},i} - I_{\text{average,hkl}}|}{\sum_{\text{hkl}} \sum_i I_{\text{hkl},i}} \times 100$.

^c $R_{\text{work}} = \frac{\sum_{\text{hkl}} |F_{\text{obs}} - F_{\text{calc}}|}{\sum_{\text{hkl}} |F_{\text{obs}}|} \times 100$. R_{free} is calculated in the same way on a subset of reflections that are not used in the refinement (5%).

^d Deviation is from ideal values.

once this molecular replacement solution were combined with low resolution (4 Å) multiple-wavelength anomalous diffraction data from a selenomethionine derivative and subjected to 4-fold averaging. The resulting electron density allowed rebuilding and refinement of the LmNADK1 tetramer using native data to 2.4 Å of resolution (Table 1). Then the structure of the second crystal form (space group I222) was solved by molecular replacement using the native structure (Table 2).

LmNADK1 is a homotetramer of approximate dimensions 100 × 60 × 50 Å (Fig. 2). In the monoclinic crystal, one tetramer was observed in the asymmetric unit and corresponds to the biological tetramer. Only one monomer is present in the orthorhombic form, and the biological tetramer was deduced from the crystallographic symmetries. The tetrameric arrangement is very similar to that described for the other NADKs and corresponds to a dimer of dimers, stabilized by large interfaces (~3500 Å²) between the C-terminal domains.

The monomer structure of LmNADK1 is very similar to one of homologues from *M. tuberculosis* and *A. fulgidus*, showing root mean square deviations of 2.2 and 2.4 Å, respectively. Nevertheless, some structural features in the C-terminal domain appeared specific to the NADKs from Gram(+) bacilli, in particular a sequence motif 188-NnrvFR-193 in the vicinity of the bound nucleobases, corresponding to a small loop absent in other NADKs (supplemental Fig. S1).

Within each monomer the polypeptide chain is organized into an N-terminal and a C-terminal domain (Fig. 2). The C-terminal domain adopts an original topology composed of two β-sheets arranged in an antiparallel 12-stranded β-sandwich. It comprises most of the motifs strictly conserved among

NADKs, including the motif 150-DG///sTPsGsTAY-163 involved in NAD recognition (27) (where/stands for any hydrophobic residue, and lowercase/capital letters are partially/strictly conserved residues, respectively) (see supplemental Fig. S1).

The N-terminal domain is composed of five β-strands and three α-helices. In LmNADK1 and in its orthologs from other Gram(+) bacteria, the N-terminal domain is shorter than in other NADKs due to the loss of the second α-helix. This domain harbors the well conserved motif GGDGT. Besides this motif, little conservation is observed, in agreement with the low level of specificity for the phosphate donor (which can be polyphosphate or any nucleoside triphosphate).

Binding of Natural Substrates to LmNADK1—To investigate the catalytic mechanism, we next tried to obtain crystal forms of LmNADK1 bound to NAD or NADP. Despite several attempts of soaking and co-crystallization with NAD or NADP, monoclinic P2₁ apo crystals failed to reveal electron density corresponding to these ligands. Soaking of NAD or NADP was finally successful with the second crystal form, I222. The ligand TAA was washed out and successfully replaced by NAD or NADP. Because apo as well as NAD and NADP-bound crystals yielded near 2-Å data sets (Table 2), the catalytic mechanism can be analyzed in more detail (supplemental Figs. S2 and S3).

Despite the change in crystal forms, the overall structures of the apoenzyme and the bound states were highly similar, with only small re-orientation of the two domains (Fig. 2) as well as of a few side chains in the substrate binding site (root mean square deviation of 0.15–0.53 Å for isolated N-terminal and C-terminal domains versus 0.47–0.75 Å for full-length chains).

TABLE 2
Data collection and refinement statistics for LmNADK1-complexes

a.u., asymmetric units.

	Wild type						D45N mutant NAD
	TAA	DTA	NAD	NADP	Ap2A	2'-p-Ap2A	
Data collection							
Space group	I222						
Cell dimension <i>a</i> , <i>b</i> , <i>c</i> (Å)	63.2, 74.6, 118.3	63.1, 75.3, 118.7	62.5, 73.5, 118.7	61.9, 77.5, 117.8	62.6, 75.9, 118.5	63.1, 75.7, 118.8	62.4, 76.4, 119.2
No. molecules in a.u.	1	1	1	1	1	1	1
Wavelength (Å)	0.9780	0.9793	0.9763	0.9340	0.9330	0.9330	0.9340
Resolution (Å) ¹	30.99-2.10 (2.21-2.10)	25.29-1.85 (1.95-1.85)	37.14-2.10 (2.21-2.10)	37.37-2.10 (2.21-2.10)	37.93-2.22 (2.34-2.22)	35.09-2.20 (2.32-2.20)	32.14-1.90 (2.00-1.90)
<i>R</i> _{merge} (%) ^{a,b}	8.2 (48.8)	6.8 (44.2)	7.1 (56.8)	7.7 (44.8)	5.4 (41.1)	4.8 (46.0)	7.1 (39.9)
<i>I</i> / <i>σI</i> ^c	18.1 (2.9)	17.3 (1.9)	17.2 (2.0)	18.1 (4.2)	22.9 (3.5)	18.6 (1.9)	20.9 (4.1)
Completeness (%) ^a	99.9 (100.0)	98.9 (93.5)	98.7 (91.3)	96.4 (98.0)	96.8 (81.2)	99.1 (94.5)	99.0 (94.0)
Redundancy ^a	5.5 (5.7)	5.2 (2.9)	6.0 (4.4)	5.9 (5.8)	4.9 (4.0)	3.2 (2.1)	6.5 (5.2)
B-wilson	28.6	27.7	37.7	25.1	38.5	38.3	23.5
Refinement							
Resolution (Å)	2.10	1.85	2.10	2.10	2.22	2.20	1.90
No. reflections	15,878	22,941	15,633	15,714	13,383	13,914	21,902
<i>R</i> _{work} / <i>R</i> _{free} (%) ^c	20.3/23.1	19.1/21.0	20.5/25.4	19.9/26.1	20.7/25.2	20.3/23.8	20.5/24.3
No. protein atoms	2,122	2,325	2,145	2,226	2,107	2,148	2,195
No. water molecules	69	154	78	124	59	54	60
Ligand type	TAA × 2	DTA	NAD	NADP	Ap2A	2'-pAPPA	NAD
B-factors (Å ²)							
Protein	22.8	33.4	40.0	22.6	35.7	41.1	24.8
Ligands	19.9	31.7	38.2	21.4	40.6	41.3	24.9
Water	26.6	37.0	43.2	23.6	37.9	39.9	26.0
Root mean square deviations ^d							
Bond lengths (Å)	0.009	0.010	0.009	0.010	0.012	0.010	0.009
Bond angles (°)	1.3	1.5	1.5	1.5	2.3	1.5	1.4

^a Values in parentheses refer to the outermost resolution shell.

^b $R_{\text{merge}} = \frac{\sum_{hkl} \sum_i |I_{hkl,i} - I_{\text{average},hkl}|}{\sum_{hkl} \sum_i I_{hkl,i}} \times 100$.

^c $R_{\text{work}} = \frac{\sum_{hkl} |F_{\text{obs}} - F_{\text{calc}}|}{\sum_{hkl} F_{\text{obs}}} \times 100$. R_{free} is calculated in the same way on a subset of reflections that are not used in the refinement (5%).

^d Deviation is from ideal values.

Substrate-assisted Catalysis of NAD Kinases

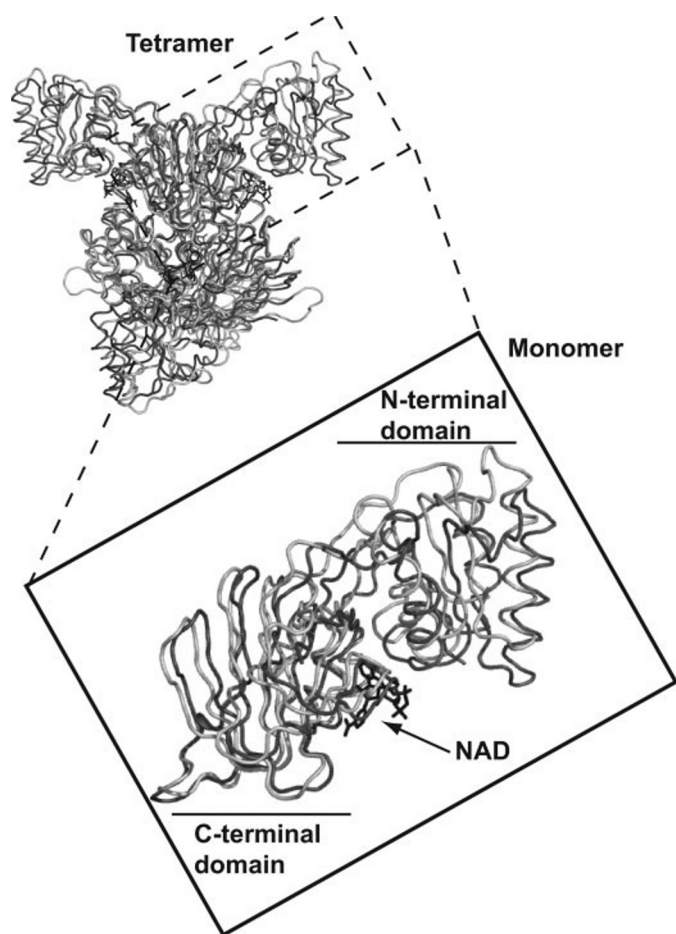


FIGURE 2. Structural superposition of the tetrameric structure of LmNADK1 in the absence (gray) and presence of NAD (black) using the C terminus as an anchor. A monomer is zoomed out to highlight the position of the NAD at the domain hinge.

As in other NADKs, the dinucleoside diphosphate binding site of LmNADK1 was formed at the interface between the two domains. The conserved motif from the N-terminal domain faces those from the C-terminal domain at the edges of the interfacial groove.

Two distinct binding pockets, named sites A and N, accommodate the adenosine and the nicotinamide ribose, respectively (supplemental Figs. S2 and S3). Although the site A is composed of residues from only one monomer, the site N includes an aspartate (Asp-150' in LmNADK1) and an alanine (Ala-185') from a second monomer.

In the site A (supplemental Figs. S2 and S3), the adenine ring is sandwiched between the side chain and the carboxylate of Ala-162 and part of the side chains of Asp-45 and Phe-74. Specific recognition of the adenine moiety involves mainly two residues: Asn-122 and Thr-161. Their side chains are hydrogen-bonded to the N6 amino group and the N7 and N3 nitrogens of the adenine. These two residues are well conserved in most NADKs and participate in an intricate hydrogen-bond network involving the neighboring side chain of Tyr-75 and the Ser-158 carboxylate. In turn, the hydroxyl of Ser-158 is also hydrogen-bonded to the hydroxyl of Tyr-75. On the contrary, few interactions are observed with the ribose moiety of adenosine beside the hydrogen bond between the Asp-45 and the 2'-hydroxyl of

NAD. Disruption of this contact in LmNADK1-NADP complex is accompanied by a slight re-orientation of the ribose (see below), whereas the 2'-phosphate group is hydrogen-bonded to the backbone of the second and third glycines of the motif ⁴³GGDGT⁴⁷.

In the site N (supplemental Figs. S2 and S3), nicotinamide binding induced only a subtle rearrangement, the small rotation of the side chain of Tyr-163. The aromatic ring of the nicotinamide stacks onto the tyrosine ring. Both the hydroxyl of this tyrosine and the amide group of the nicotinamide are hydrogen-bonded to a conserved Asp-150' from another subunit, as observed in other NADKs (15, 16). The amide group of the nicotinamide forms additional hydrogen bonds with the main-chain carbonyl of Ala-185' and the side chain of Ser-166. Recognition of the ribose attached to the nicotinamide is ensured by three hydrogen bonds through its 2' and 3'-hydroxyl groups with the side chains of Asn-122 and Asp-123. This network of interactions ensures that the other natural dinucleoside diphosphate compound, FAD, will not enter the site N.

Although the recognition of the nucleobase moieties is made through various interactions, few contacts are observed between the protein and the two phosphate groups of the NAD molecule. The diphosphate link (group linking the nucleosides) is solvent-exposed and showed alternating conformations with significant mobility. Only one histidine (His-223) was hydrogen-bonded to one of the two phosphate groups (supplemental Fig. S2). The ribose of the adenosine moiety is also rather solvent-exposed. This raised the question of the basis for the specific 2' phosphorylation of NAD by NADKs.

The Role of the Conserved GGDGT Motif—The conserved GGDGT motif of NADKs has been suggested to be catalytically important and to be involved in nucleotide binding (28) or in phosphate transfer (15).

Previous sequence comparisons had revealed that the conserved motif GGDGT of NADKs corresponds to a consensus signature /d/////gGdgs, which is well conserved in four kinase families: NAD kinases, sphingosine kinases, eukaryotic diacylglycerol kinases, and PFKs (28). PFKs phosphorylate D-fructose 6-phosphate using ATP as a phosphodonor (29) (EC 2.7.1.11; Pfam PF00365). From the crystal structure of PFKs, it was deduced that in the consensus sequence, glycines interact with the phosphates of the phospho donor (ATP) and the second conserved aspartate is involved in chelation of the catalytic dication to activate the phospho donor (29). Using our crystal structure, we performed structural comparison between the NADK-NAD and PFK-ATP complexes. It revealed that the two-domain organization of NADKs was reminiscent to those of PFKs. In both cases the active site lies at the hinge separating the two domains. However, the C-terminal domains of NADKs and PFKs adopt two distinct architectures, whereas the N-terminal domains adopt a very similar fold (70 C α s from their N-terminal domains superimpose with a root mean square deviation of 3.5 Å) (Fig. 3). Nevertheless, in PFKs and NADKs, the common GGDGT motif is similarly positioned at the two-domain interface, suggesting a similar role in catalysis.

Surprisingly, in NADKs, the central aspartate is oriented in an opposite direction, incompatible with its role in PFKs (Fig.

3). Because this position is conserved in NADKs from *M. tuberculosis* and *A. fulgidus*, these data suggest that even if NADKs and PFKs belong to the same superfamily, their enzymatic mechanisms differ.

The conformation of Asp-45 varies slightly between apo-, NADP-, and NAD-bound states of LmNADK1. In the unbound LmNADK1 structure or in the presence of the reaction product NADP, the Asp-45 of the GGDGT motif is hydrogen-bonded to three backbone amide groups that belong to residues 73–75 whose side chains are involved in adenine binding. In contrast, in LmNADK1-NAD the side chain of Asp-45 becomes hydrogen-bonded to 2'-hydroxyl group of NAD and two NADK backbone amide groups (residues 74–75). This rearrangement (supplemental Fig. S3) is accompanied by a concomitant change in the orientation of the ribose of the adenosine moiety (relative to its nucleobase).

To investigate the role of Asp-45, we determined the crystal structure of the LmNADK1-D45N mutant using the I222 TAA-bound crystal form. After washing and soaking with NAD, 2.2-Å data could be collected from these crystals (Table 2). The mutant structure showed only minor changes, and its active site was similar to that of the wild-type enzyme with the ligand present in the same conformation (see supplemental Fig. S4). The asparagine adopted the same buried conformation as the aspartate but did not form any hydrogen bond with NAD.

The mutation D45N resulted in a 10-fold decrease in activity (Table 3). Asp-45 appears clearly as a key residue for the catalytic activity of LmNADK1. This central and buried aspartate seems to have a structural role, but at the same time it may also participate in the catalysis by attracting the hydrogen of the 2'-hydroxyl group. This role may be essential for the specificity of the catalyzed phosphorylation. Indeed, the neighboring 3' hydroxyl is solvent-exposed with no direct contact with the protein, and it remains unreactive.

In most known kinases, including PFKs, conserved and catalytic acidic residues activate Mg^{2+} -ATP directly, priming it for the phosphate transfer. In contrast, our results show that in NADKs, the corresponding aspartate (Asp-45 in LmNADK1) cannot fulfill this role. The absence of other conserved acidic residue in the vicinity of the substrate suggested that a distinct reaction mechanism was involved. This raised the question of the presence of an activator of the phosphodonor and of a chelation site for the required di-cation.

Ligand Recognition and Reaction Specificity—Our results so far showed that the specific position of Asp-45 led to its interaction with the 2'-hydroxyl of NAD rather than with the diphosphate link. The absence of strong recognition between the diphosphate groups of NAD and NADKs led us to suggest the rational design of new ligands. Various linkers might be used as a replacement for the phosphate groups to bridge the two nucleobases of NAD. We synthesized 5'-thioadenosine (TA, Fig. 1C) and its *S*-acetylated form (TAA, Fig. 1C) as precursors of NAD mimics. The structures of LmNADK1 in complex with each of these adenosine analogues (Table 2) showed few variations compared with the unbound structure and to those in complex with NAD or NADP. Surprisingly, these compounds bind in a dimeric form in the NAD binding site of LmNADK1 and occupy both sites A and N. In both complexes, the adenosine scaffold, which occupied the site A, is oriented like the adenosine moiety of NAD. The second adenosine perfectly mimics the nicotinamide and its ribose and

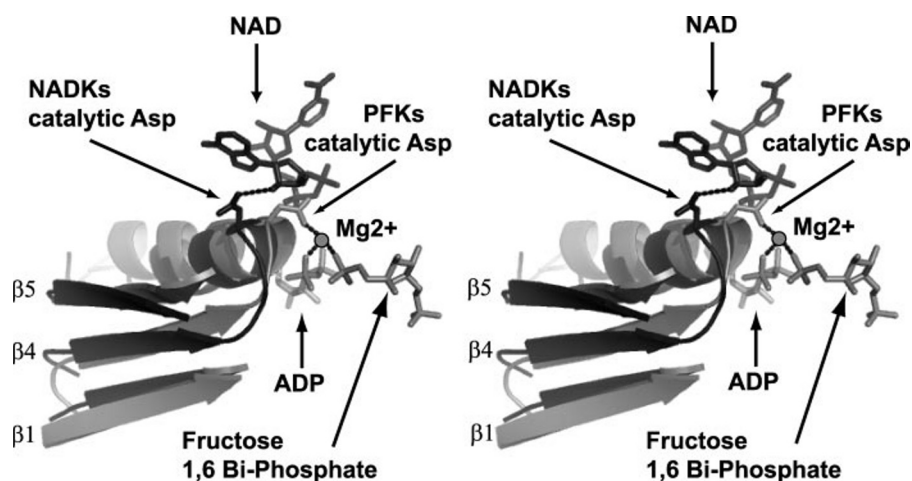


FIGURE 3. Stereo view of the superposed N-terminal domains of NADKs and PFKs. The N termini of LmNADK1 and *E. coli* PFK were superposed using the program ViTO (33). The picture was generated by the program PYMOL. Gray and black schematics and wireframes represent *E. coli* PFK/ADP/FBP/ Mg^{2+} and LmNADK1/NAD, respectively.

TABLE 3

Kinetic parameters of LmNADK1 and its variants D45N

The kinetic values are presented as mean \pm S.E. for three independent determinations. WT, wild type.

Substrate	Protein	ATP	V_{max}^a	K_m	$S_{0.5}$	n_H	k_{cat}^b	k_{cat}/K_m	$k_{cat}/S_{0.5}$
		mM		mM	mM		s^{-1}	s^{-1}/mM	s^{-1}/mM
ATP	WT ^c		6.67 \pm 0.9	2.8 \pm 0.01			13.78 \pm 1.86	4.92	
	D45N ^c		0.98 \pm 0.16	2.1 \pm 0.4			2.03 \pm 0.33	0.97	
NAD	WT ^d	4.0	6.35 \pm 0.75		1.11 \pm 0.01	1.27 \pm 0.06	13.12 \pm 1.55		11.8
		0.5	1.75 \pm 0.30		0.71 \pm 0.16	1.62 \pm 0.21	3.62 \pm 0.64		5.1
	D45N ^d	4.0	0.65 \pm 0.12		1.05 \pm 0.19	1.02 \pm 0.06	1.34 \pm 0.25		1.28
		0.5	0.20 \pm 0.01		0.50 \pm 0.06	1.78 \pm 0.39	0.41 \pm 0.02		0.82

^a μ mol of NADP/mg of protein/min.

^b Assuming that the molecular mass of the tetramer (with His tag) is 124 kDa.

^c Data for 10 various ATP concentrations at three various NAD concentrations for three enzymatic preparations (obtained by fitting the data to the Michaelis-Menten equation $v = V_m[ATP]/K_m + [ATP]$).

^d Kinetic parameters were obtained by fitting data to the Hill equation ($v = V_m[NAD]^n/S_{0.5}^n + [NAD]^n$) and determined for a fixed ATP concentration of 4.0 or 0.5 mM.

Substrate-assisted Catalysis of NAD Kinases

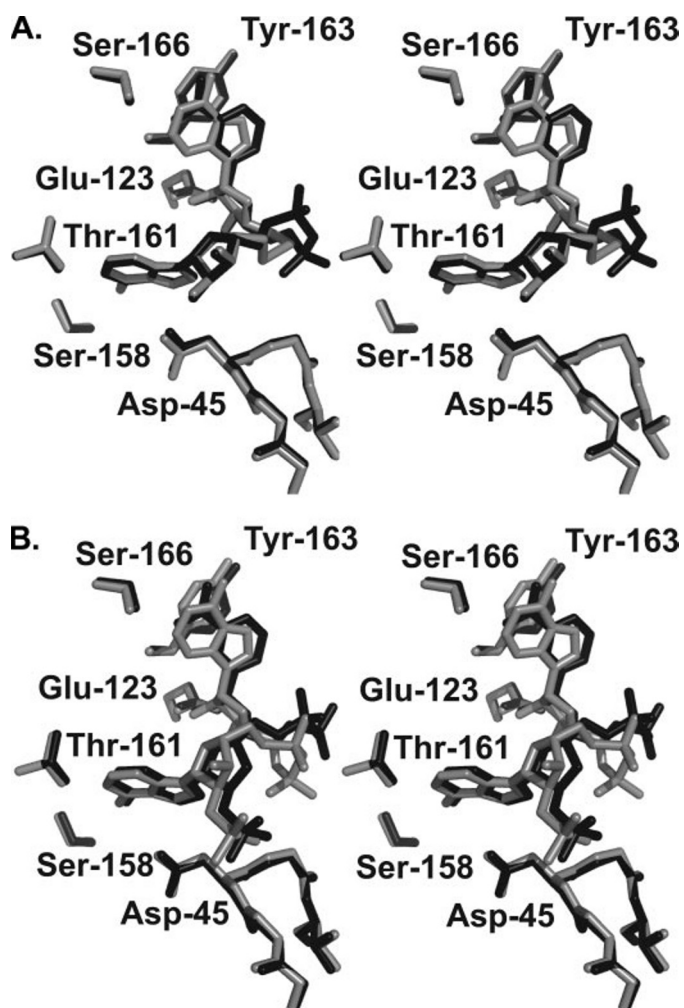


FIGURE 4. *A*, stereo view of the superposition of LmNADK1-NAD (black) and LmNADK1-DTA (gray) active site. *B*, stereo view of the superposition of LmNADK1-NADP (black) and LmNADK1-2'-p-Ap2A (gray) active site.

showed very similar interactions with the protein despite the change of ring nature (supplemental Fig. S5). Compared with NAD, only slight differences were observed in the relative orientation of the nucleobases and a small shift in the position of the water molecule bridging them. The crystal complexes showed that acetyl groups of TAAs point toward each other (distance S5'-S5', ~5 Å), whereas in the deprotected form (thioadenosine) a disulfide bridge (distance S5'-S5', 2.0 Å) covalently linked the compound into a dimer named di-5'-thioadenosine (*DTA*, Fig. 1C and supplemental Fig. S5). This latter might have formed in solution in the absence of reductant. In conclusion, the dimerization of 5'-thioadenosine appeared to have mimicked a complete natural dinucleotide substrate.

Enzymology experiments confirmed the competitive inhibition by these two synthetic compounds with K_i values of 3.6 and 0.02 mM for TAA and DTA, respectively. These affinities are low but similar to those observed for the natural ligands NAD ($K_m \sim 1$ mM) and NADP ($K_i \sim 0.04$ mM). Intriguingly, the two novel inhibitors possessed a 2'-hydroxyl readily accessible for phosphorylation by LmNADK1. Furthermore, the ribose moieties occupy strictly identical

positions in the NAD- and DTA-bound crystal structures (see Fig. 4A). However, no phosphotransfer in presence of ATP could be observed (data not shown). This prompted us to synthesize a closer mimic of both DTA and NAD (Ap2A, Figs. 1B and 4B and supplemental Fig. S6) to investigate the role of the phosphate groups in catalysis and the potential impact of the nucleobase substitution.

The structure of Ap2A bound to LmNADK1 was also solved to a resolution of 2.2 Å (Table 2). It showed that the new ligand adopted a conformation highly similar to that of DTA and perfectly mimicked NAD. Moreover, in the structure solved after crystal soaking with both Ap2A and Mg^{2+} -ATP, a clear density corresponding to Ap2A bearing a 2' phosphate group was observed (2'-phospho-Ap2A (2'-p-Ap2A), Fig. 1B, and supplemental Fig. S6), inferring that Ap2A could be used as a substrate by LmNADK1, in contrast to TAA and the closely related DTA.

These results revealed that the presence of a correctly oriented 2'-hydroxyl in DTA is not sufficient for the catalysis to occur. Moreover, the presence of the diphosphate groups of the substrate seems to be important. Even though we failed to identify electron density for bound metal ions (Mg^{2+} or Mn^{2+}), this suggested that the negatively charged phosphates might be involved in the di-cation chelation.

To evaluate the putative substrate-assisted catalysis, a new directed mutation was performed. The histidine 223 is the only residue whose side chain transiently interacts with the phosphate groups (see above). This histidine was mutated to glutamate to introduce a negatively charged residue. The glutamate was predicted to be able to chelate a di-cation. This mutant was twice less active than the wild type (0.47 versus 1.1 units/mg) on the biologically relevant substrate NAD. On the contrary, its activity toward DTA was increased 2-fold (from 0.13 to 0.24 units/mg). The crystal structure of the mutant H223E explained the low activity, because the glutamate side chain folded back in a buried position. Glu-223 forms hydrogen bonds with its own backbone nitrogen and the side chain of the histidine 53 (data not shown), preventing a higher impact on catalysis. However, the observed change in the ratio of enzyme activity on NAD versus DTA for the wild-type and the mutant enzymes confirmed the proposed substrate-assisted mechanism.

This mechanism would explain the low di-cation specificity and at the same time provide the molecular basis for specific productive recognition of dinucleotide-diphosphate substrates.

DISCUSSION

NADKs from Gram(+) bacteria represent a promising novel therapeutic target for a whole spectrum of human pathogens including bacilli and staphylococci. Here, we have determined the crystal structures of NADK from *L. monocytogenes* in the free state and bound to NAD, NADP, and two non-natural ligands.

In contrast to the previously reported complexes of NADK-NADP and NADK-NADs from *M. tuberculosis* and *A. fulgidus* (15, 16), all our structures were determined at near 2 Å of resolution, allowing a more detailed analysis of the changes

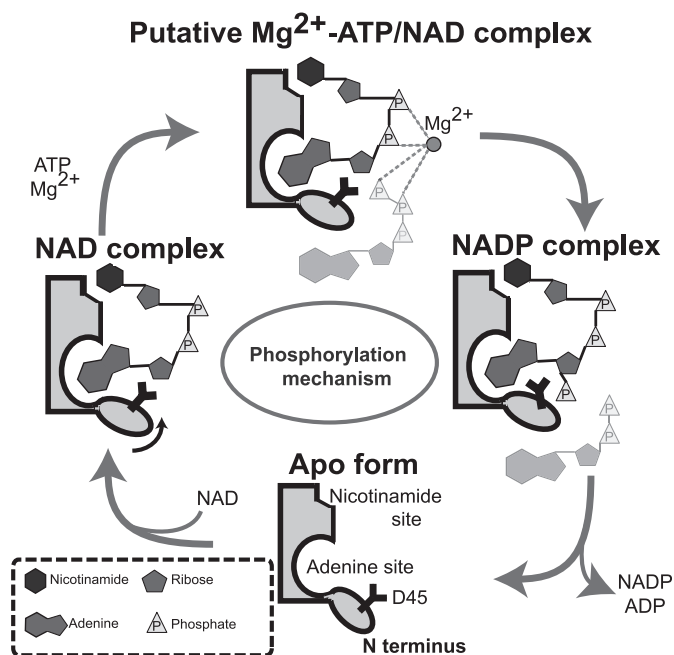


FIGURE 5. **Schematic flow of the reaction of NAD phosphorylation.** The substrate-assisted catalysis mechanism proposed for NADKs (see "Discussion") implies chelation of the catalytic di-cation Mg^{2+} by both the phosphate group of the donor and the diphosphate group of the substrate. Protein domains are drawn as filled shapes with thick lines. The catalytic aspartate 45 is drawn as a thick Y symbol. The ligands observed in the various crystal structures are drawn as plain shapes, whereas shaded forms correspond to the phosphate donor and the di-cation placed at their putative positions.

accompanying the catalytic reaction. This is especially true for the aspartate of the conserved motif GGDGT. Our analysis revealed that the aspartate of the conserved GGDGT motif has a different catalytic role in PFKs and NADKs. In PFKs this conserved residue is involved in ATP activation, whereas in NADK it is involved in NAD activation.

Indeed, based on these structures in combination with site-directed mutagenesis and enzymology experiments, we propose that in NADKs, the conserved aspartate is involved in proton abstraction from the 2'-hydroxyl of NAD to activate the phospho-acceptor. This explains why NADK phosphorylates only the 2'-hydroxyl of adenosine and not the functionally equivalent 3'-hydroxyl. In addition, our results infer that the diphosphate group of the substrate plays the role of a di-cation chelator, revealing a mechanism involving substrate-assisted catalysis (Fig. 5). Together, these two aspects of this mechanism would cooperatively ensure the specificity of the catalyzed reaction. Thus, our results yield important insights into the specificity and mechanism of the catalytic action of NADKs.

Nevertheless, this mechanism might be extended to the families of diacylglycerol/sphingosine kinases (30, 31). The first structure (PDB code 2JGR) of a member (YegS) of this protein family was recently solved (32). Structural comparison highlighted that the aspartate of the well conserved GGDGT motif adopts the same position (supplemental Fig. S7). In this structure, a pyrophosphate group interacts with residues from the GGDGT motif (mainly the last glycine and the threonine). It potentially mimics the phosphate donor. However, in both NADKs and the related lipid kinases, the precise orientation of

the phosphate donor and/or the position of the catalytic di-cation remain presently unresolved.

As a first step toward designing new inhibitors for LmNADK1, we have described herein the structural and enzymatic characterization of two novel compounds mimicking NAD, namely Ap2A and DTA, the latter representing a novel synthetic inhibitor for NADK. Building tighter links between the two nucleobases would lead to more efficient inhibitors.

Acknowledgments—We thank O. Barzu and A.-M. Gilles (Institut Pasteur, Paris), C. Royer, C. Roumestand, F. Hoh, and C. Frauer (Centre de Biochimie Structurale, Montpellier) for helpful discussions and technical help.

REFERENCES

- Pucci, M. J. (2006) *Biochem. Pharmacol.* **71**, 1066–1072
- Gerdes, S. Y., Scholle, M. D., D'Souza, M., Bernal, A., Baev, M. V., Farrell, M., Kurnasov, O. V., Daugherty, M. D., Mseeh, F., Polanuy, B. M., Campbell, J. W., Anantha, S., Shatalin, K. Y., Chowdhury, S. A., Fonstein, M. Y., and Osterman, A. L. (2002) *J. Bacteriol.* **184**, 4555–4572
- Kobayashi, K., Ehrlich, S. D., Albertini, A., Amati, G., Andersen, K. K., Arnaud, M., Asai, K., Ashikaga, S., Aymerich, S., Bessieres, P., Boland, F., et al. (2003) *Proc. Natl. Acad. Sci. U. S. A.* **100**, 4678–4683
- Suzuki, N., Okai, N., Nonaka, H., Tsuge, Y., Inui, M., and Yukawa, H. (2006) *Appl. Environ. Microbiol.* **72**, 3750–3755
- Sasseti, C. M., Boyd, D. H., and Rubin, E. J. (2003) *Mol. Microbiol.* **48**, 77–84
- Thanassi, J. A., Hartman-Neumann, S. L., Dougherty, T. J., Dougherty, B. A., and Pucci, M. J. (2002) *Nucleic Acids Res.* **30**, 3152–3162
- Zalacain, M., Biswas, S., Ingraham, K. A., Ambrad, J., Bryant, A., Chalker, A. F., Iordanescu, S., Fan, J., Fan, F., and Lunsford, R. D. (2003) *J. Mol. Microbiol. Biotechnol.* **6**, 109–126
- Grose, J. H., Joss, L., Velick, S. F., and Roth, J. R. (2006) *Proc. Natl. Acad. Sci. U. S. A.* **103**, 7601–7606
- Kawai, S., Mori, S., Mukai, T., Suzuki, S., Yamada, T., Hashimoto, W., and Murata, K. (2000) *Biochem. Biophys. Res. Commun.* **276**, 57–63
- Lerner, F., Niere, M., Ludwig, A., and Ziegler, M. (2001) *Biochem. Biophys. Res. Commun.* **288**, 69–74
- Schomburg, I., Chang, A., Ebeling, C., Gremse, M., Heldt, C., Huhn, G., and Schomburg, D. (2004) *Nucleic Acids Res.* **32**, 431–433
- Garavaglia, S., Galizzi, A., and Rizzi, M. (2003) *J. Bacteriol.* **185**, 4844–4850
- Kawai, S., Mori, S., Mukai, T., Hashimoto, W., and Murata, K. (2001) *Eur. J. Biochem.* **268**, 4359–4365
- Garavaglia, S., Raffaelli, N., Finaurini, L., Magni, G., and Rizzi, M. (2004) *J. Biol. Chem.* **279**, 40980–40986
- Liu, J., Lou, Y., Yokota, H., Adams, P. D., Kim, R., and Kim, S. H. (2005) *J. Mol. Biol.* **354**, 289–303
- Mori, S., Yamasaki, M., Maruyama, Y., Momma, K., Kawai, S., Hashimoto, W., Mikami, B., and Murata, K. (2005) *Biochem. Biophys. Res. Commun.* **327**, 500–508
- Pignot, M., Pljevaljcic, G., and Weinhold, E. (2000) *Eur. J. Org. Chem.* **3**, 549–555
- (1994) *Acta Crystallogr. D Biol. Crystallogr.* **50**, 760–763
- Weeks, C. M., and Miller, R. (1999) *Acta Crystallogr. D Biol. Crystallogr.* **55**, 492–500
- Bricogne, G., Vornrhein, C., Flensburg, C., Schiltz, M., and Paciorek, W. (2003) *Acta Crystallogr. D Biol. Crystallogr.* **59**, 2023–2030
- Cowtan, K. (1994) *Newsletter on Protein Crystallography* **31**, 34–38
- McCoy, A. J., Storoni, L. C., and Read, R. J. (2004) *Acta Crystallogr. D Biol. Crystallogr.* **60**, 1220–1228
- Jones, T. A., Zou, J. Y., Cowan, S. W., and Kjeldgaard, M. (1991) *Acta Crystallogr. A* **47**, 110–119
- Emsley, P., and Cowtan, K. (2004) *Acta Crystallogr. D Biol. Crystallogr.* **60**, 2126–2132

Substrate-assisted Catalysis of NAD Kinases

25. Winn, M. D., Isupov, M. N., and Murshudov, G. N. (2001) *Acta Crystallogr. D Biol. Crystallogr.* **57**, 122–133
26. Moffatt, J. G. A. (1964) *Can. J. Chem.* **42**, 599–604
27. Raffaelli, N., Finaurini, L., Mazzola, F., Pucci, L., Sorci, L., Amici, A., and Magni, G. (2004) *Biochemistry* **43**, 7610–7617
28. Shirakihara, Y., and Evans, P. R. (1988) *J. Mol. Biol.* **204**, 973–994
29. Labesse, G., Douguet, D., Assairi, L., and Gilles, A. M. (2002) *Trends Biochem. Sci.* **27**, 273–275
30. Taha, T. A., Hannun, Y. A., and Obeid, L. M. (2006) *J. Biochem. Mol. Biol.* **39**, 113–131
31. Topham, M. K. (2006) *J. Cell Biochem.* **97**, 474–484
32. Bakali, M. A., Dolores Herman, M., Johnson, K. A., Kelly, A., Wieslander, A., Hallberg, B. M., and Nordlund, P. (2007) *J. Biol. Chem.* **282**, 19644–19652
33. Catherinot, V., and Labesse, G. (2004) *Bioinformatics* **20**, 3694–3696